Research Square

Preprints are preliminary reports that have not undergone peer review.
They should not be considered conclusive, used to inform clinical practice,
or referenced by the media as validated information.

# Dry-out characteristics of flat-plate pulsating heat pipe for proton exchange membrane fuel cell cooling

**Yuyang Li**

czuliyy@cczu.edu.cn

Changzhou University

**Kai Zheng**

Changzhou University

**Enhai Liu**

Changzhou University

**Ming Peng**

Changzhou University

**Yecheng Liu**

Changzhou University

**Zhixiang Xing**

Changzhou University

**Research Article**

**Keywords:**

**Posted Date:** November 5th, 2026

**DOI:** https://doi.org/10.21203/rs.3.rs-10990843/v1

**License:** This work is licensed under a Creative Commons Attribution 4.0 International License.
Read Full License

**Additional Declarations:** No competing interests reported.

# Dry-out characteristics of flat-plate pulsating heat pipe for proton exchange membrane fuel cell cooling

Yuyang Li*, Kai Zheng*, Enhai Liu, Ming Peng, Yecheng Liu, Zhixiang Xing
Changzhou University, Changzhou 213164, China

**Abstract:** When flat-plate pulsating heat pipe is integrated for the cooling of proton exchange membrane fuel cell (PEMFC), excessively high temperatures at the evaporator section and insufficient liquid working fluid reflux can induce localized dry-out in partial channels. Aiming at the operating temperature range of the PEMFC, the dry-out characteristic of the flat-plate pulsating heat pipe was investigated. The results reveal that the flat-plate CLPHP exhibits no thermal runaway with increasing heating power at the initial stage of dry-out. Under this condition, the maximum temperature difference of the PEMFC is only 3.77 ℃ with a temperature variance of 8.30 ℃$^2$, indicating a favorable temperature uniformity. As the dry-out degree intensifies, the proportion of liquid working fluid in the evaporator section decreases, the liquid slugs and thick liquid film gradually vanish, and the flow pattern transitions from slug flow to semi-annular flow and annular flow, which degrades heat transfer efficiency.

**Keywords:** PEMFC; Flat-plate CLPHP; Dry-out performance; Vapor-liquid flow; Temperature uniformity

| **Nomenclature** | | $\rho$ | Density [kg/m$^3$] |
|---|---|---|---|
| $D$ | Diameter [m] | Subscripts | |
| $R$ | Thermal resistance [°C/W] | li | Liquid |
| $U$ | Voltage [V] | va | Vapor |
| $I$ | Current [A] | i | Inner |
| $l$ | Length [m] | min | Minimum |
| $T$ | Temperature [K] | max | Maximum |
| $A$ | Area [m$^2$] | hy | Hydraulic diameter |
| $V$ | Volume [m$^3$] | es | Evaporator section |
| $Q_{\text{in}}$ | Heat input [W] | as | Adiabatic section |
| $k$ | Thermal conductivity [W/m·K] | cs | Condenser section |
| $Eo$ | Loránd Eötvös | eq | Equivalent |
| $Bo$ | Bond number | fil | Filling |
| Greek symbols | | tot | Total |
| $\sigma$ | Surface tension [N/m] | eff | Efficient |
| $g$ | Gravity acceleration [m/s$^2$] | | |

## 1 Introduction

A PEMFC possesses numerous merits including freedom from Carnot cycle limitations, high specific energy and specific power, rapid cold-start capability at low temperatures, and zero emissions [1,2]. At present, the PEMFC has been applied in various fields such as automobiles [3], aviation [4], and submarines [5]. Nevertheless, while a PEMFC generates electric power, approximately half of its input energy is converted into waste heat [6]. If heat accumulates inside a PEMFC without timely dissipation, the overall cell temperature will rise. Excessively high

temperature will trigger dehydration of the proton exchange membrane and a sharp drop in proton conductivity. In severe cases, thermal degradation and mechanical failure of the membrane material may even occur, bringing about potential safety hazards [7-9]. However, an excessively low temperature of a PEMFC slows down the electrochemical reaction kinetics and reduces catalyst activity. Meanwhile, water produced at the cathode cannot be efficiently discharged, thereby triggering water flooding [10-12]. Therefore, large heat generation, a narrow optimal operating temperature range, and difficult temperature regulation of a PEMFC constitute one of the bottlenecks restricting its practical application. With the industrialization of a PEMFC, an efficient and stable cooling system is of vital importance. At present, the mature cooling method for a PEMFC relies on forced convection heat transfer using liquid coolant [13-15]. Nevertheless, the liquid coolant possesses low sensible heat, which results in large coolant flow rates and a significant temperature difference between the inlet and outlet of the stack. The parasitic power consumption for liquid pumping is considerable, accounting for 5–10 % of the power generated by a PEMFC [16]. In addition, such a cooling system features complicated structure and extremely stringent sealing requirements. Meanwhile, a PEMFC imposes strict limitations on ionic impurities contained in the coolant, further raising the overall system cost [17].

To address the drawbacks of liquid coolant adopted for cooling a PEMFC, a phase change cooling scheme based on a flat-plate pulsating heat pipe is proposed. A flat-plate pulsating heat pipe is manufactured from high thermal conductivity metal, with liquid working fluid filled in its internal channels. It achieves rapid heat transfer via high temperature boiling and low temperature condensation of the working fluid. As a gas-liquid two-phase flow system integrating sensible heat transfer, phase change heat transfer, and expansion work, and covering multiple disciplines and various parameters, it is recognized as a thermal superconductor [18,19]. Compared with the conventional liquid coolant cooling technique, a flat-plate pulsating heat pipe possesses a simple and compact structure, causes no corrosion to a PEMFC and produces no ions. It presents a small temperature difference among vapors within the evaporator section and excellent isothermal performance, rendering it one of the most promising passive cooling approaches for a PEMFC to date [20,21]. During the operation of a PEMFC, the ability to maintain its ideal operating temperature and temperature uniformity mainly depends on the evaporation, boiling, gas-liquid two-phase flow and condensation of the working fluid inside a flat-plate pulsating heat pipe of the cooling system, which constitute the core factors determining its heat transfer performance. Accordingly, investigating the local dry-out characteristics at the evaporator section of a flat-plate pulsating heat pipe under the operating temperature range of a PEMFC, maintaining the reflux of liquid working fluid in the evaporator section, and thereby sustaining the normal gas-liquid two-phase flow of a flat-plate pulsating heat pipe from the evaporator section through the adiabatic section to the condenser section are of remarkable practical significance for improving the efficient heat transfer of a flat-plate pulsating heat pipe under high heat flux density at the evaporator section and further realizing effective cooling of a PEMFC [22-24].

A pulsating heat pipe is generally arranged vertically, with its evaporator section located at the bottom. Driven by expansion work and gravity assistance, the liquid working fluid flows back to the evaporator section to form an efficient heat transfer cycle. Local dry-out occurring at the evaporator section of a pulsating heat pipe is usually induced by high heat flux density in the evaporator. This leads to an elevated temperature on the channel surface and thinning of the liquid film on the channel wall. In extreme cases, the channel wall directly contacts the vapor working

fluid, resulting in a sharp temperature rise of the evaporator section and triggering local dry-out [25,26]. Slobodeniuk et al. [27] milled square serpentine channels on a molybdenum substrate and charged ethanol with a filling ratio of 40 % as the working fluid to investigate the influence of gas-liquid interface oscillation on internal flow patterns inside a flat-plate pulsating heat pipe under microgravity conditions. The results reveal that when the heating power of the evaporator section increases from 100 W to 150 W, the evaporator temperature rises significantly with a temperature increment of 36 ℃. This phenomenon indicates that liquid working fluid accumulates in the condenser section of a flat-plate pulsating heat pipe and can hardly flow back to the evaporator section. The insufficient supply of liquid working fluid in the evaporator leads to dry-out, and the heat transfer cycle cannot be sustained. Liu et al. [28] investigated the local dry-out characteristics of a pulsating heat pipe charged with ethanol under various heat transfer distances via visual experiments, and further made a comparison with a water-based pulsating heat pipe. The experimental results show that the dry-out performance is closely related to the flow regime of the working fluid, and the stagnation of liquid flow constitutes the primary cause for local dry-out in the evaporator section. Compared with the water-based one, ethanol with lower surface tension exhibits superior anti-dry-out performance, especially under a long heat transfer distance. Palani et al. [29] adopted a two-dimensional transient pressure-based Navier-Stokes solver combined with the SIMPLE algorithm to predict field variables. The standard $k-\varepsilon$ model with wall treatment was employed to capture turbulent physical processes, and the VOF model was used to simulate gas-liquid two-phase flow characteristics. They investigated the dry-out limit of a pulsating heat pipe filled with water at a filling ratio of 50 %. The results reveal that the adiabatic section acts as a functional pressure buffer barrier between the evaporator section and the condenser section. The vapor pressure in the evaporator section changes slowly, which can delay the occurrence of dry-out. Krambeck et al. [30] machined chamfers to form grooves with an angle of 29.1 ± 2.9 ° inside the channels at the bends of the evaporator section of a copper flat-plate pulsating heat pipe. The lateral grooves act as artificial nucleation sites to facilitate bubble nucleation of the liquid working fluid in the evaporator section. Meanwhile, they function as capillary structures to promote the backflow of liquid working fluid. The liquid working fluid can cover the channel surface of the evaporator section in the form of liquid slugs and liquid films, which delays the onset of dry-out and increases the critical dry-out heat flux of the evaporator section of a pulsating heat pipe. Liu et al. [31] developed a two-phase heat and mass transfer model describing liquid film dynamics in a pulsating heat pipe and carried out localized visual experiments. The results indicate that R1336mzz (Z) generates a larger driving force accompanied by lower flow resistance compared with water and ethanol as working fluids for a pulsating heat pipe. This increases the oscillating velocity of vapor-liquid working fluid inside a pulsating heat pipe. At high flow velocities, the flow pattern of vapor-liquid working fluid can transform from reciprocating oscillating flow to unidirectional circulating flow, thereby preventing the occurrence of local dry-out in the evaporator section. Li et al. [32] developed a model capable of capturing the core physical mechanisms of a pulsating heat pipe. The model describes the temporal evolution of liquid film length and thickness as well as their correlation with heat transfer. It can predict the dry-out phenomenon in the evaporator section of a pulsating heat pipe under a heating power of 40 W. The results demonstrate that dry-out is directly associated with the length and thickness of the liquid film within the evaporator section, and latent heat of phase change dominates the heat transfer process of a pulsating heat pipe.

Nevertheless, at the present stage, few systematic investigations focus on the local dry-out

characteristics at the evaporator section of a flat-plate pulsating heat pipe charged with binary non-azeotropic mixtures under the operating temperature range of a PEMFC. Visual research concerning the boiling of liquid working fluid and the reflux process of liquid slugs and liquid films inside rectangular channels of the evaporator section under high heat flux density is still in its infancy. Moreover, limited studies have been conducted on the coupled comparative analysis of the evolution of internal temperature, pressure and thermal resistance as well as gas-liquid two-phase flow patterns inside a flat-plate pulsating heat pipe under local dry-out conditions. The research group has previously investigated the influencing mechanisms of key parameters including working fluid type and filling ratio on the heat transfer performance of a flat-plate pulsating heat pipe via non-visual and visual experimental methods [33,34]. On this basis, this paper adopts non-visual tests for temperature and pressure measurement and high-speed imaging visual tests to systematically explore the intrinsic correlation between the variations in internal temperature, pressure, and heat transfer thermal resistance, and the gas-liquid flow state of a rectangular channel flat-plate pulsating heat pipe. The heat pipe is charged with a binary non-azeotropic mixed working fluid of methanol and deionized water at a mass ratio of 5:1, and the investigation is conducted under high heating power conditions with and without local dry-out in the evaporator section. This study reveals the local dry-out mechanism of a flat-plate pulsating heat pipe, providing theoretical support for the optimized application of a flat-plate pulsating heat pipe in the thermal management of a PEMFC.

## 2 Experimental setup

The experiments consist of two parts including non-visual acquisition of temperature and relative pressure, and visual image capturing. The experimental setup mainly comprises a non-visual flat-plate pulsating heat pipe and a visual flat-plate pulsating heat pipe, vacuum and liquid charging system, electric heating system, data acquisition system, cooling system, and image recording system. The schematic diagram of the experimental setup is shown in Fig. 1.

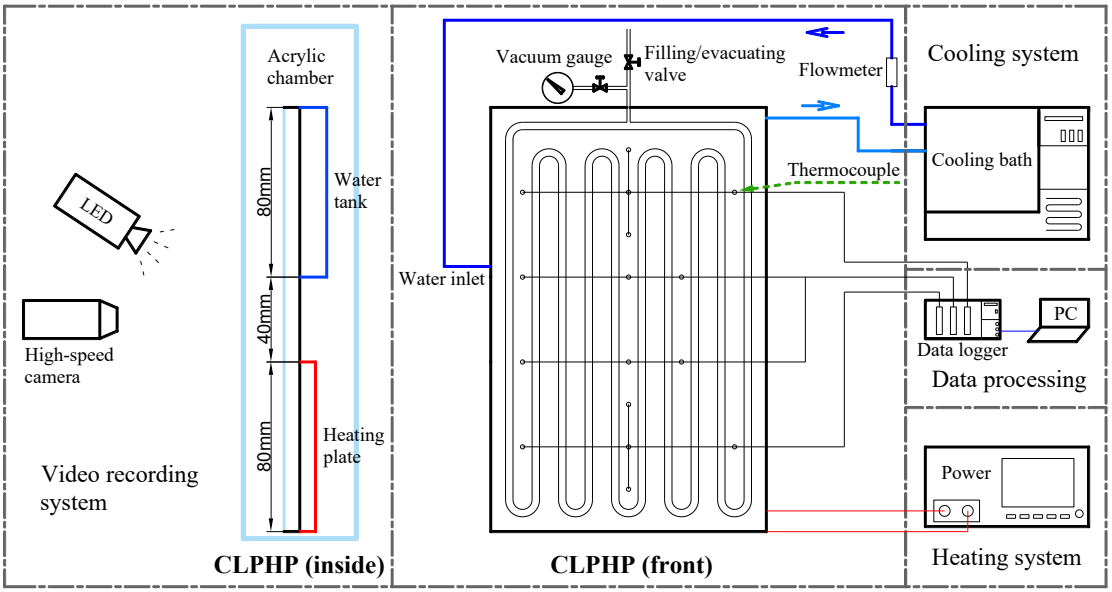



Fig. 1. Schematic of flat-plate pulsating heat pipe experimental setup

The motion of vapor-liquid working fluid inside a pulsating heat pipe is primarily governed by the combined effects of gravity and surface tension. If the inner diameter is excessively large, the surface tension cannot sustain the stable vapor-liquid slug structure within the channels, resulting

in liquid interface rupture and spontaneous coalescence. When the inner diameter is too small, the gravitational effect weakens and surface tension becomes dominant, hindering the flow of internal working fluid. The relationship between surface tension and gravity can be characterized by the dimensionless $Eo$ [35]:

$$Eo = \frac{(\rho_{\mathrm{li}} - \rho_{\mathrm{va}}) g D_{\mathrm{i}}^2}{\sigma} = Bo \tag{1}$$

The theoretical hydraulic diameter for the successful startup and stable operation of a pulsating heat pipe needs to satisfy the following equation [36]:

$$0.7\sqrt{\frac{\sigma}{g(\rho_{\mathrm{li}} - \rho_{\mathrm{va}})}} = D_{\min} \le D_{\mathrm{hy}} \le D_{\max} = 2\sqrt{\frac{\sigma}{g(\rho_{\mathrm{li}} - \rho_{\mathrm{va}})}} \tag{2}$$

A non-visual flat-plate pulsating heat pipe is fabricated by bonding a 6061 aluminum alloy plate of 200 × 110 × 1.5 $mm^3$ and a thin plate of the same alloy with identical length and width but a thickness of 0.4 mm. Rectangular channels with a cross-section of 2.3 × 1.1 $mm^2$ are machined on the surface of the aluminum alloy plate, with a total of 9 turns. the flat-plate pulsating heat pipe is arranged vertically. The heights of the evaporator section, adiabatic section and condenser section are 80 mm, 40 mm and 80 mm, respectively. The evaporator section closely contacts a copper plate embedded with four ceramic heating sheets of matching dimensions. The copper plate is heated by a DC power supply with constant power output to simulate heat generation of a PEMFC. A water tank is fixed on the outer surface of the condenser section, and cooled deionized water with an inlet temperature set to 20 ℃ circulates inside the groove. A flowmeter (LZJ-10, accuracy 2.5 %) is installed on the inlet pipeline of the water tank, and thermocouples (TT-T-30, accuracy 0.5 ℃, the same thermocouple model is adopted hereinafter) are arranged at both the inlet and outlet. Five thermocouples are installed at the half-thickness position of the copper heating plate. Five thermocouples are arranged in the evaporator section and the condenser section of the flat-plate pulsating heat pipe, respectively. Three thermocouples are separately placed at the junction between the condenser section and the adiabatic section, as well as the junction between the adiabatic section and the evaporator section, as shown in Fig. 1. Each thermocouple is embedded into a micro-hole with a depth of 0.8 mm to reduce temperature measurement errors. Thermocouple signals are acquired by a data logger (Hioki 8423, accuracy 0.01 ℃) at a sampling interval of 5 s, and the average values are adopted to reduce temperature measurement errors.

In the visual experimental system, high borosilicate glass with a thickness of 2 mm is used to replace the 0.4 mm thick aluminum alloy thin plate for the flat-plate pulsating heat pipe. Both the heating plate and cooling water tank are halved compared with those in the non-visual system. To minimize heat loss, all surfaces of the non-visual and visual flat-plate pulsating heat pipes, except the high borosilicate glass surface, are insulated with thermal cotton. The visual flat-plate pulsating heat pipe is placed inside a transparent acrylic box to suppress natural and forced convection of ambient air. Visual images are captured by a high-speed CCD camera (NPX-GS650UM, maximum frame rate of 10000 fps).

Prior to each test, a vacuum pump (SHZ-DIII, the maximum vacuum degree is 0.98 MPa) is utilized to evacuate the setup, which minimizes the thermal resistance induced by non-condensable gases. Afterwards, the flat-plate pulsating heat pipe is kept stationary in a relatively enclosed environment for 24 h under pressure holding to examine its air tightness. The working fluid is charged into the flat-plate pulsating heat pipe by virtue of the pressure difference between the

internal and external surroundings, and the internal pressure is measured by a vacuum pressure gauge (Y60BF, accuracy 2.5 %). Filling ratio ($FR$):

$$FR = \frac{V_{\text{fil}}}{V_{\text{tot}}} \tag{3}$$

A flat-plate pulsating heat pipe under steady heat transfer conditions relies primarily on sensible heat via forced convection of internal vapor-liquid slugs and latent heat from vapor-liquid phase change for thermal energy transport. Its heat transfer capacity greatly exceeds that of pure metals, so it is referred to as a heat superconductor. The thermal resistance $R$ of the flat-plate pulsating heat pipe can be calculated by the following formula (the average value of data at 10 time points under steady-state conditions is adopted to minimize measurement errors):

$$R = \frac{1}{10}\frac{\sum_{i=1}^{10}\left(\overline{T_{\text{es}}} - \overline{T_{\text{cs}}}\right)_{\text{i}}}{Q_{\text{in}}} \tag{4}$$

Where, the heat input $Q_{\text{in}}$ can be expressed as:

$$Q_{\text{in}} = U_{\text{eff}} \cdot I_{\text{eff}} \tag{5}$$

The equivalent thermal conductivity $Q_{\text{in}}$ of the flat-plate pulsating heat pipe can be calculated as:

$$k_{\text{eq}} = \frac{l_{\text{eff}}}{RA_{\text{cs}}} \tag{6}$$

Where, the effective length $l_{\text{eff}}$ of the flat-plate pulsating heat pipe is given by:

$$l_{\text{eff}} = \frac{1}{2}(l_{\text{es}} + l_{\text{cs}}) + l_{\text{as}} \tag{7}$$

Five thermocouples are installed in the evaporator section and condenser section of the flat-plate pulsating heat pipe, respectively, and their average values are used to represent the temperature of each section. The average temperatures of the evaporator and condenser sections can be calculated by the following equations:

$$\overline{T_{\text{es}}} = \frac{1}{5}\sum_{i=1}^{5} T_{\text{esi}} \tag{8}$$

$$\overline{T_{\text{cs}}} = \frac{1}{5}\sum_{i=1}^{5} T_{\text{csi}} \tag{9}$$

The binary non-azeotropic mixture consisting of methanol (purity ≥99.5 %) and deionized water with a mass ratio of 5:1 is adopted as the working fluid in the experiment. The phase diagrams illustrating the variations of different molar fraction ratios with temperature and relative pressure are shown in Fig. 2(a) and 2(b), respectively. The mixture of methanol and deionized water is a miscible, non-azeotropic binary solution exhibiting positive deviations. At a fixed temperature, the liquidus lines of methanol-deionized water mixture under different relative pressures versus molar fraction ratios lie slightly above the liquidus line of an ideal mixture, also known as the Raoult line, which is a straight line. During vapor-liquid phase transition, a larger positive deviation of the mixed solution corresponds to a greater concentration difference between the vapor and liquid phases, leading to a more distinct vapor-liquid phase transition sequence [37]. As can be seen from the phase diagram, the methanol-deionized water mixture exhibits obvious temperature and concentration shifts within the vapor-liquid phase transition zone. Methanol has a lower boiling point than deionized water. As the temperature of the evaporator section of the flat-plate pulsating heat pipe

rises, methanol in the binary working fluid boils and vaporizes first. Consequently, the concentration of methanol in the vapor phase gradually increases, while the proportion of deionized water in the liquid phase continuously rises. Therefore, when local dry-out occurs with increasing evaporator temperature of the flat-plate pulsating heat pipe, deionized water becomes the dominant liquid-phase working fluid inside the channel. Compared with methanol, deionized water possesses higher surface tension, which hinders the backflow of liquid working fluid and further aggravates the severity of dry-out.

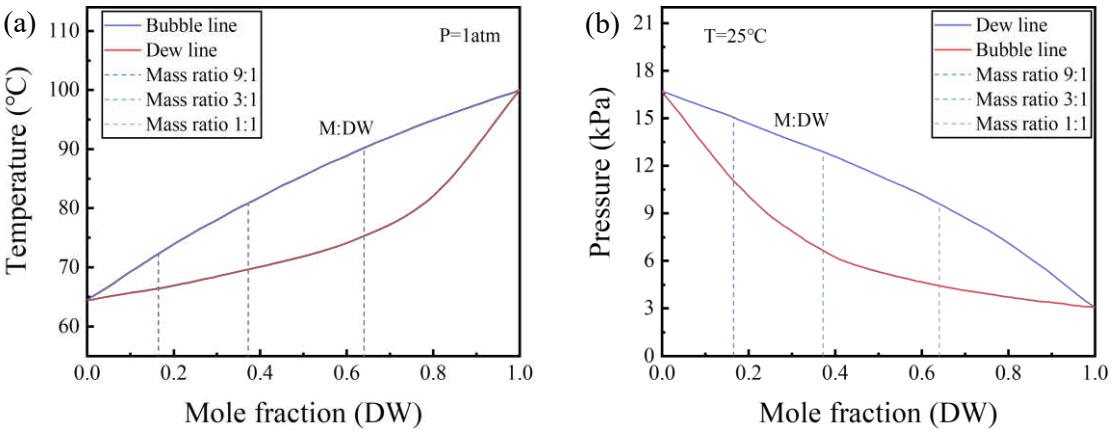



Fig. 2. Phase diagrams of M:DW. (a) Temperature-mole fraction; (b) Pressure-mole fraction

## 3 Results and discussion

3.1 Thermal conductivity of flat-plate pulsating heat pipe

Taking the average temperature of the evaporator section of flat-plate pulsating heat pipe as the independent variable, fitting equations for thermal conductivity corresponding to the integral and segmented thermal resistances of flat-plate pulsating heat pipe are established separately based on experimental data, as illustrated in Fig. 3(a) and 3(b). From the startup of heat transfer to the occurrence of local dry-out in the evaporator section of flat-plate pulsating heat pipe, the variation trends of thermal conductivity for the integral structure and each section of the segmented structure with evaporator temperature $T_{es}$ all conform to the GaussMod equation.

Among them, the fitting equation of integral thermal resistance (Fit_tot) shows a small deviation from the experimental results (Exp_tot), with a goodness of fit $Rsq$ of 0.9943, which indicates high confidence.

$$k_{tot} = -0.28 + 1.88 \times e^{0.007-\frac{T_{es}-46.01}{88.75}\times \mathrm{erf}\left(\frac{z}{1.41}\right)+1} \qquad RSq = 0.9943 \tag{10}$$

$$double(z) = \frac{T_{es} - 46.01}{10.75} - 0.12 \tag{11}$$

Essential differences exist in the internal heat transfer mechanisms of the channels in the evaporator, adiabatic and condenser sections of flat-plate pulsating heat pipe, leading to significant discrepancies in thermal conductivity among each section. Based on experimental data, thermal conductivity fitting equations as functions of the average evaporator temperature are developed for the evaporator section (Fit_es), adiabatic section (Fit_as) and condenser section (Fit_cs) of the flat-plate pulsating heat pipe, respectively. The thermal conductivity of each section of the flat-plate pulsating heat pipe exhibits identical variation trends with rising temperature, and all fitting equations for sectional thermal conductivity achieve high goodness of fit values.

Thermal conductivity of the evaporator section $k_{es}$:

$$k_{es} = -1.28 + 2.75 \times e^{0.006-\frac{T_{es}-40.61}{151.46}\times \mathrm{erf}\left(\frac{z}{1.41}\right)+1} \qquad RSq = 0.9754 \tag{12}$$

$$double(z) = \frac{T_{es} - 40.61}{16.52} - 0.11 \tag{13}$$

Thermal conductivity of the adiabatic section $k_{as}$:

$$k_{as} = -0.36 + 2.08 \times e^{0.014-\frac{T_{es}-48.06}{60.22}\times \mathrm{erf}\left(\frac{z}{1.41}\right)+1} \qquad RSq = 0.9818 \tag{14}$$

$$double(z) = \frac{T_{es} - 48.06}{10.19} - 0.17 \tag{15}$$

Thermal conductivity of the condenser section $k_{cs}$:

$$k_{cs} = 1.03 + 0.88 \times e^{0.008-\frac{T_{es}-51.16}{51.21}\times \mathrm{erf}\left(\frac{z}{1.41}\right)+1} \qquad RSq = 0.9818 \tag{16}$$

$$double(z) = \frac{T_{es} - 51.16}{6.28} - 0.12 \tag{17}$$

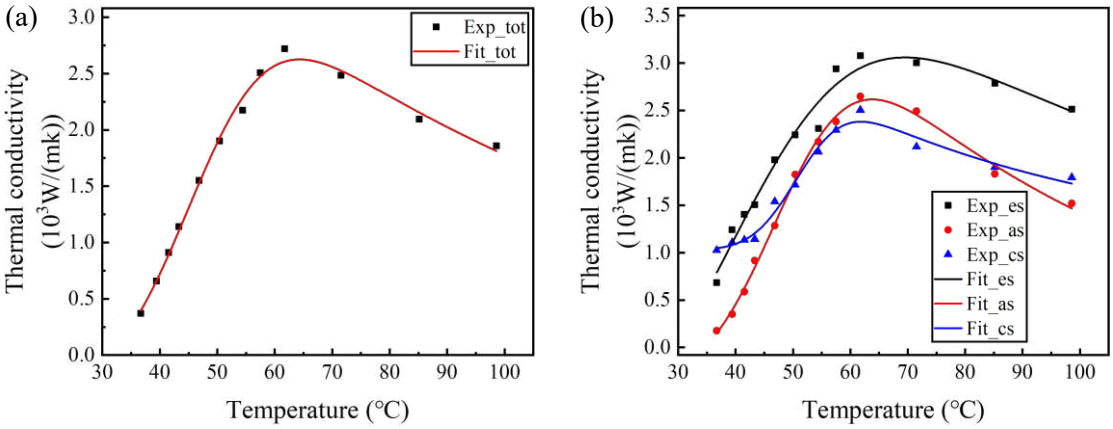



Fig. 3. Comparison between experimental data and fitted results for thermal conductivity of flat-plate pulsating heat pipe: (a) integral; (b) segmented

3.2 Local dry-out characteristics of flat-plate pulsating heat pipe

As the heating power of the heating plate simulating heat generation from PEMFC increases, the temperature of the heating plate rises rapidly, as shown in Fig. 4. When the heating power increases from 0 W to 20 W, the temperature rises from 25.40 ℃ to 41.54 ℃, and the thermal resistance of the flat-plate pulsating heat pipe drops sharply from 1.543 ℃/W to 0.631 ℃/W. Nevertheless, with further elevation of heating power, the growth rate of temperature slows down, and the thermal resistance of the flat-plate pulsating heat pipe decreases at a reduced rate. This indicates that the flat-plate pulsating heat pipe completes heat transfer startup at a heating power of 20 W. The internal liquid working fluid boils and vaporizes to form gas-liquid two-phase flow, which improves the heat transfer efficiency.

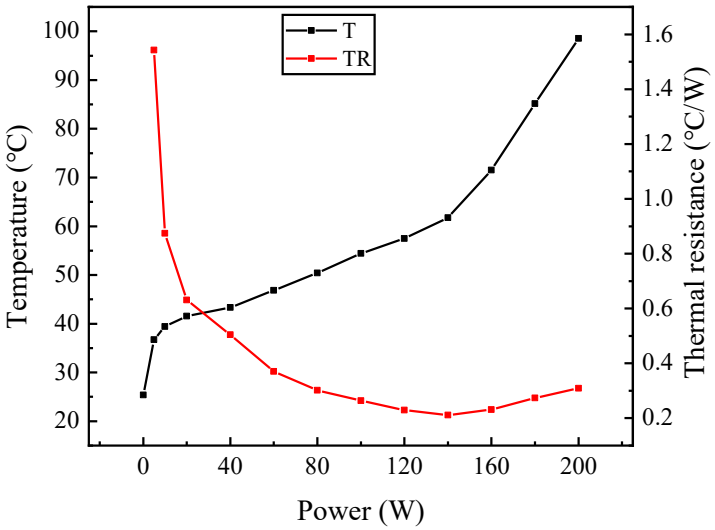



Fig. 4. Variation curves of temperature and thermal resistance with heating power

As the heating power applied to the evaporator section of the flat-plate pulsating heat pipe rises to 140 W, it can be observed from the figure that further increases in heating power alter the temperature evolution from steady growth to accelerated growth. The slope of temperature versus heating power increases from 0.21 ℃/W within the 120–140 W range to 0.49 ℃/W for 140–160 W, representing a 133.3 % rise in slope magnitude. Meanwhile, the thermal resistance curve of the flat-plate pulsating heat pipe shifts from a gradual declining trend to a gradual rising trend once the heating power exceeds 140 W. This phenomenon indicates that local dry-out occurs in the evaporator section of the flat-plate pulsating heat pipe when the heating power exceeds 140 W. Under such conditions, the liquid working fluid cannot flow back sufficiently, and the channel wall of the evaporator section lacks a continuous liquid film coverage. The inner wall of partial evaporator channels is thus in direct contact with the vapor-phase working fluid. Given the low specific heat capacity of vapor, the vapor cannot absorb sufficient heat to stabilize the evaporator temperature under continuous heat input from the heat source. As a result, the temperature rise rate accelerates, which further exacerbates the local dry-out.

Pulsating flow with vapor-liquid slugs exists inside the flat-plate pulsating heat pipe. Nevertheless, pulsation is mainly observed in the adiabatic and condenser sections at high heating powers. The wall temperature of the evaporator section remains relatively high, so the reflux liquid film is rapidly heated and vaporized upon entering this region. The wall temperature rises closer to the evaporator elbow. Moreover, the fluid flow direction changes abruptly at the elbow, generating intensified flow disturbances that facilitate bubble nucleation and accelerate vaporization rates. Accordingly, the total vapor volume and vapor generation rate within the channels increase remarkably. This weakens the pulsatile driving force and gravitational force acting on the vapor-liquid slugs, thereby obstructing the backflow of liquid working fluid. Sustained and extensive insufficient supply of liquid working fluid in the evaporator section breaks the heat balance of the evaporator, which leads to a sharp temperature rise, increased thermal resistance and deteriorated heat transfer in the flat-plate pulsating heat pipe evaporator. Nevertheless, no dramatic rise in thermal resistance or severe heat transfer failure occurs at the initial stage of dry-out. Accordingly, the flat-plate pulsating heat pipe integrated with PEMFC possesses a certain safety margin and favorable operational safety.

The internal relative pressure of the flat-plate pulsating heat pipe rises progressively with

increasing heating power of the evaporator section, and its variation trend conforms to the two-exponential decay model, as shown in Fig. 5. When the heating power exceeds 140 W and local dry-out emerges inside the flat-plate pulsating heat pipe, the growth rate of internal relative pressure accelerates with rising heating power. As discussed in the previous section, further aggravation of dry-out speeds up the temperature rise and accelerates the vaporization rate of liquid working fluid in the evaporator section. Liquid slugs or liquid films vaporize rapidly once they flow back into the evaporator. This drastically raises the volume fraction of vapor-phase working fluid inside the flat-plate pulsating heat pipe and reduces the proportion of liquid-phase working fluid, which ultimately causes a rapid drop in internal relative pressure. However, the vapor-liquid flow channels inside the flat-plate pulsating heat pipe are fabricated by laminating two thin plates. A lower internal relative pressure enables tighter contact between the thin plates and yields more stable flow channels. In contrast, when the internal relative pressure rises gradually and even exceeds 0 kPa, this value is above atmospheric pressure. The contact tightness between the two thin plates degrades. This causes vapor and liquid working fluids to cross-communicate between adjacent channels, which brings a risk of channel structural damage.

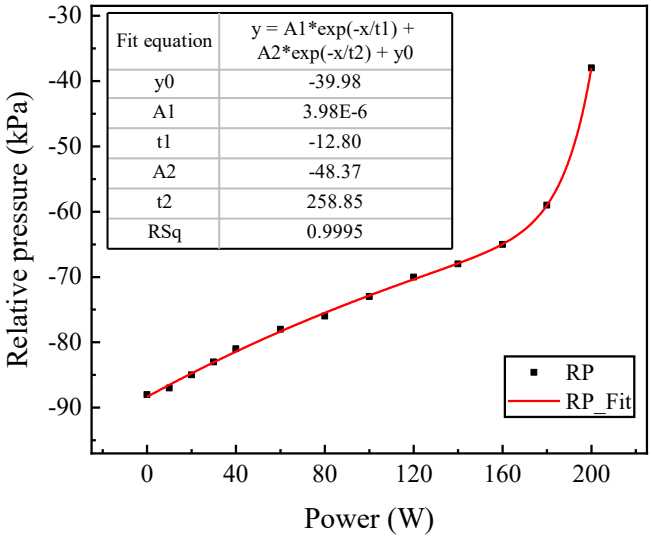



Fig. 5. Variation curve of internal relative pressure with heating power

3.3 Analysis of temperature uniformity with and without local dry-out

The performance and service life of PEMFC rely heavily on temperature regulation. The PEMFC not only requires a relatively high ideal operating temperature range, but more crucially, demands uniform temperature distribution. Local hotspots or uneven temperature gradients inside the PEMFC can induce inconsistent performance across different regions of the membrane electrode assembly, resulting in disordered current distribution. This intensifies cyclic dry-wet stress on partial membrane regions and accelerates material degradation. Meanwhile, non-uniform temperature distribution gives rise to unbalanced thermal and water management. Water accumulation easily occurs in low-temperature zones while membrane dry-out takes place in high-temperature zones, thereby creating a vicious cycle.

As shown in Fig. 6, when the flat-plate pulsating heat pipe operates under stable heat transfer at a heating power of 140 W, the average temperature of the heating plate simulating heat generation of PEMFC reaches 71.51 °C. The maximum temperature appears at the bottom of the heating plate, and the temperature difference between the bottom and the top where the minimum temperature is

measured is 3.18 ℃. The temperature variance RSq of the five temperature measurement points is 5.85 ℃². At a heating power of 200 W, the average temperature of the heating plate rises to 98.56 ℃. The temperature climbs rapidly after the onset of dry-out, yet no uncontrollable continuous temperature surge is observed. The relative magnitude and distribution position of temperatures remain consistent with those under stable heat transfer at a heating power of 140 W. The maximum temperature difference between the highest and lowest temperature points reaches 3.77 ℃, which is 0.58 ℃ higher than the maximum temperature difference measured under stable heat transfer. The temperature variance RSq of the five temperature measurement points is 8.30 ℃², representing an increment of 2.45 ℃² compared with the stable heat transfer condition. At the initial stage of local dry-out in the evaporator section of flat-plate pulsating heat pipe, only insufficient liquid supply occurs in partial regions of the evaporator. The reflux liquid slugs or liquid films are rapidly heated and vaporized by the inner walls of flow channels. Nevertheless, liquid working fluid intermittently flows back to the evaporator section along channel inner walls. Meanwhile, liquid films attached to the inner walls of adiabatic sections flow back to the evaporator section under gravity. Such liquid backflow maintains the efficient heat transfer capacity of the pulsating heat pipe and prevents a sharp and unstable temperature rise in the evaporator section. Accordingly, relatively stable temperature and favorable temperature uniformity can still be maintained after the occurrence of dry-out inside flat-plate pulsating heat pipe, which guarantees uniform temperature distribution and stable operation of PEMFC.

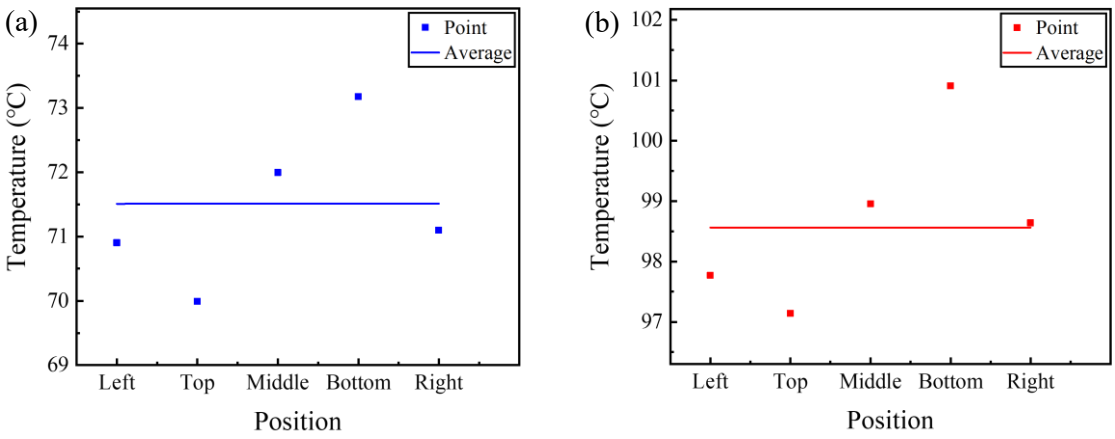



Fig. 6. Comparison of PEMFC temperature uniformity before and after dry-out

3.4 Visualization analysis of local dry-out

Heat transfer of flat-plate pulsating heat pipe primarily via internal working fluid latent heat of phase change and forced convection sensible heat. Local dry-out in the evaporator section is manifested as the rapid vaporization of liquid slugs or liquid films on the inner walls of evaporator channels under high temperature. The liquid working fluid fails to fully cover the channels, which results in direct contact between channel walls and vapor-phase working fluid, and further leads to a substantial temperature rise in the evaporator section. Fig. 7 presents visualized comparisons of vapor-liquid working fluid inside evaporator channels of flat-plate pulsating heat pipe as heating power rises gradually from 100 W to 160 W. The figure reveals the evolution of vapor-liquid working fluid and corresponding flow patterns inside the evaporator from stable heat transfer to the onset of local dry-out. It can be clearly observed from the figure that the volume fraction of liquid working fluid inside channels decreases sequentially with rising heating power, and the flow regime

gradually transforms from slug flow to semi-annular flow and annular flow. At a heating power of 100 W, intense nucleate boiling of liquid working fluid occurs at the bottom of elbow 1 and elbow 2, generating abundant bubbles. Liquid slugs exist in channels on the right side of elbow 3 and elbow 4, as well as channels on the left side of elbow 5. Distinct thick liquid films flow back along channel walls in the gravity direction within channels on the right side of elbow 3 and the left side of elbow 5. However, at a heating power of 160 W for the evaporator section of flat-plate pulsating heat pipe, almost no liquid slugs or thick liquid films can be found. Vapor-phase working fluid occupies most space inside the evaporator section, liquid coverage on elbows declines, and there is a phenomenon where the liquid working medium has already vaporized completely before it can return to the elbow.

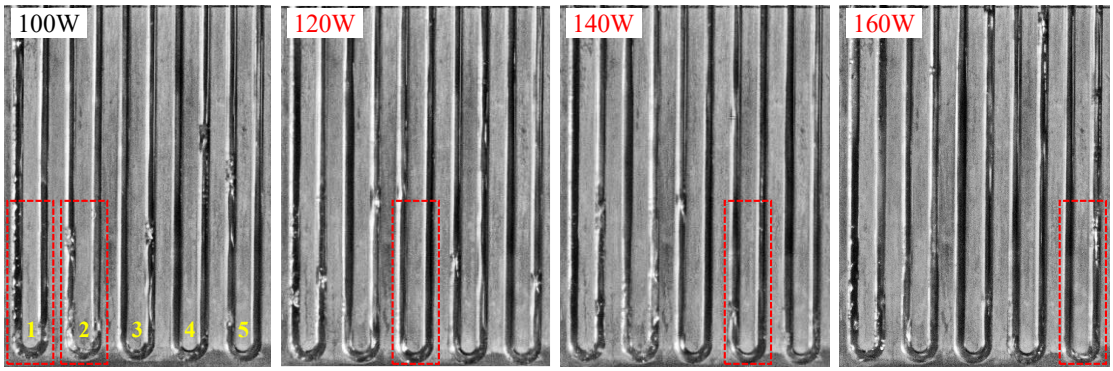



Fig. 7. Visual comparison of local dry-out evolution in evaporator section

Fig. 8 shows visualized experimental comparisons of partially enlarged elbows and channels in the evaporator section of flat-plate pulsating heat pipe. The comparison covers elbow 3 under stable heat transfer at 100 W, as well as elbow 1 and elbow 3 under local dry-out at 160 W. It can be seen from the figure that at a heating power of 160 W, no liquid slugs or thick liquid films exist in the two channels around elbow 1. Only several scattered static tiny droplets adhere to the inner surface of the visual glass. In contrast to the backflow of thick liquid films and nucleate boiling of liquid working fluid at elbow 1 under 100 W, the liquid-vapor phase change ratio at elbow 1 drops drastically under the higher heating power of 160 W, which substantially reduces heat transfer efficiency. The comparison at elbow 3 exhibits more obvious differences. Under stable heat transfer at a heating power of 100 W, slug flow appears on the right side of elbow 3, and liquid-vapor phase change via nucleate boiling can be clearly observed at the elbow bottom. In contrast, when local dry-out occurs at 160 W, the bottom of elbow 3 is not covered by thick liquid films or liquid slugs, and no boiling of liquid working fluid is detected. Only thin liquid films cover the left-side channels, leading to a remarkable decline in heat transfer efficiency compared with the 100 W condition.

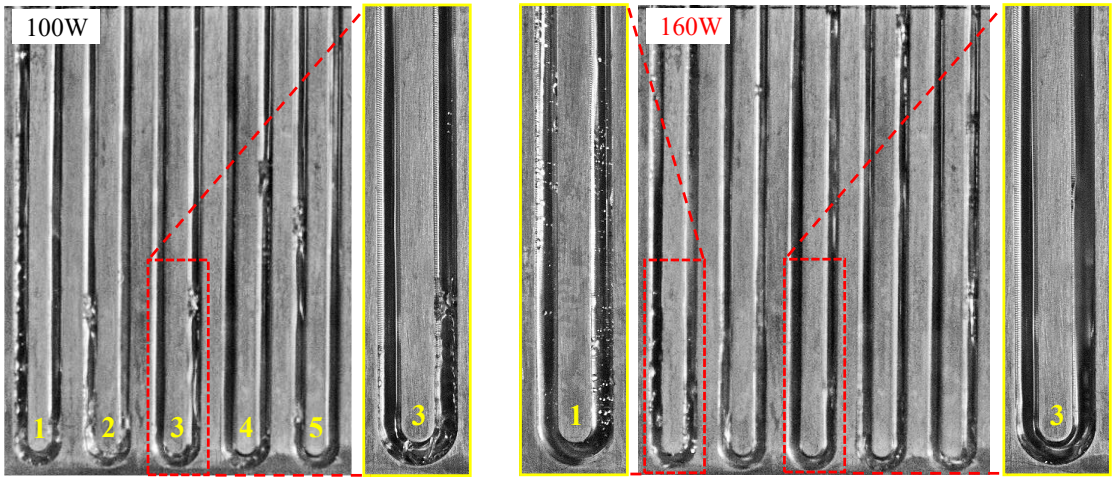



Fig. 8. Visual comparison of the evaporator section with and without local dry-out

Therefore, local dry-out in flat-plate pulsating heat pipe is a relative concept, rather than a state where all liquid working fluid inside the evaporator section is completely vaporized. The flat-plate pulsating heat pipe in this work serves primarily as a heat transfer medium. Accordingly, the onset of dry-out for flat-plate pulsating heat pipe is defined as the turning point where thermal resistance stops decreasing and begins rising with increasing heating power. This criterion is adopted to investigate dry-out characteristics and corresponding heat transfer performance of flat-plate pulsating heat pipe. This research provides valuable guidance for suppressing or eliminating dry-out and preventing abrupt temperature surges in flat-plate pulsating heat pipe.

## 4 Conclusions

Based on the operating temperature range of PEMFC, non-visual experiments are conducted to investigate the heat transfer performance of flat-plate pulsating heat pipe under stable heat transfer and local dry-out conditions in the evaporator section. Visual comparative analysis is performed to characterize vapor-liquid flow patterns and working fluid states inside evaporator channels with and without local dry-out. The main conclusions are drawn as follows:

1) The evolution trends of thermal conductivity corresponding to integral and segmented thermal resistance of flat-plate pulsating heat pipe both fit the GaussMod equation. At the initial stage of dry-out, the thermal resistance of flat-plate pulsating heat pipe does not rise sharply, which avoids continuous and unstable temperature growth of PEMFC and guarantees favorable operational safety.

2) When local dry-out emerges in the evaporator section of flat-plate pulsating heat pipe, the maximum temperature difference on the heating plate simulating PEMFC heat generation is merely 3.77 ℃ with a temperature variance of 8.30 ℃². The device exhibits excellent temperature uniformity, which supports the efficient and stable operation of PEMFC.

3) Visual comparison results of local dry-out reveal that aggravated dry-out reduces the volume fraction of internal liquid working fluid. Liquid slugs and thick liquid films inside channels gradually diminish and eventually disappear entirely, and the two-phase flow pattern transforms from slug flow to semi-annular flow and annular flow.

## Acknowledgement

This study benefits from the financial support by the General Program of Basic Research for Institutions of Higher Education in Jiangsu Province (Grant No. 25KJB620002) and the Changzhou Science and Technology Program (Grant No. CJ20250028).

## References


[1] Sun X L, Xi D X, Fu J Q, et al. Boosted deep neural network model for forecasting the electrochemical impedance of a proton exchange membrane fuel cell under varying operating conditions[J]. Renewable Energy, 2026, 256.

[2] Bu W X, Liang H, Gu W, et al. Multi-criteria evaluation of symmetric tesla-like valve flow channel geometry on proton exchange membrane fuel cell performance using analytic hierarchy process-entropy weight method[J]. Energy Conversion and Management, 2026, 350.

[3] Kebede G A, Wang F K, Woldegiorgis B H. A prediction method with uncertainty-aware for the remaining useful life and state of health of the proton exchange membrane fuel stack[J]. Journal of Power Sources, 2026, 663.

[4] Schröder M, Gentner C, Ansar S A. Advanced air supply system topologies for fuel cells in aircraft applications[J]. Energy Conversion and Management, 2026, 350.

[5] Zhou K H, Zhang G H, Bai H F, et al. The flight verification of an integrated propulsion system powered by PEMFCs with direct airflow intake design[J]. Applied Energy, 2025, 377.

[6] Li R H, Wu Z Z, He G R, et al. A novel architecture for enhanced thermal management in fuel cell cooling systems[J]. Energy, 2026, 344.

[7] Yang K, Wang B W, Gong Z C, et al. Temperature collaborative control strategy using dung beetle optimizer in proton exchange membrane fuel cell system[J]. Renewable Energy, 2026, 256.

[8] Li W H, Li S, Du C Q, et al. A deep reinforcement learning control method for PEMFC thermal management and air supply system[J]. Applied Thermal Engineering, 2025, 279.

[9] Luo Y, Ali M A H, Ghazali N N N, et al. Modeling and simulation of a novel thermal management strategy and temperature distribution in PEMFC[J]. Applied Thermal Engineering, 2025, 274.

[10] El Idi M M, Ankouni M, Slama R B, et al. Critical review of the latest advances in thermal management techniques for PEM fuel cells[J]. Renewable & Sustainable Energy Reviews, 2026, 226.

[11] Song K, Hou T Z, Jiang J H, et al. Thermal management of liquid-cooled proton exchange membrane fuel cell: A review[J]. Journal of Power Sources, 2025, 648.

[12] Hu H, Xu J, Qiu Y, et al. Multi-physics collaborative optimization of high current density PEMFC with micro-encapsulated phase change material suspension using EWM-TOPSIS and machine learning[J]. Fuel, 2027, 428.

[13] Su H Y, Xu H S, Wang L, et al. A review on thermal management strategy for liquid-cooling proton exchange membrane fuel cells: Temperature regulation and cold start[J]. Applied Energy, 2025, 393.

[14] Huang T M, Zou P T, Xiao Y F, et al. Comprehensive analysis of half-wave continuous cooling channels in performance of proton exchange membrane fuel cells[J]. International Journal of Heat and Mass Transfer, 2025, 244.

[15] Wang Z K, Wang Y, Yuan X L, et al. Design and thermal management of proton exchange membrane fuel cells with biomimetic spider web cooling[J]. Applied Thermal Engineering, 2026, 289.

[16] Cui W X, Li X H, Zhang P J, et al. Hydrogen burners for the cold start process of hydrogen fuel cells[J]. Journal of Power Sources, 2025, 629.

[17] Deng Z J, Liu K X, Xing S, et al. Optimization of cathode channel design, bolt torque, and assembly mode for enhanced performance in air-cooled proton exchange membrane fuel cells[J]. International Journal of Hydrogen Energy, 2025, 102: 702-14.

[18] Hu Y, Meng G Y, Yao Y C, et al. Experimental investigation on the start-up and thermal performance of nanofluid-based pulsating heat pipe[J]. Applied Thermal Engineering, 2025, 259.
[19] Brede C, Heubeck A, Czwielong F, et al. Thermal performance of cost-effective extruded aluminum pulsating heat pipes for electronic system cooling[J]. International Journal of Heat and Mass Transfer, 2026, 254.
[20] Nazari M A, Ahmadi M H, Blazek V, et al. Performance enhancement of oscillating heat pipes by structural modification: A comprehensive review[J]. Sustainable Energy Technologies and Assessments, 2025, 75.
[21] Patel E D, Shukla A K, Kumar S. Thermal performance of concentrically arranged two interconnected single-loop pulsating heat pipes[J]. Energy Conversion and Management, 2025, 323.
[22] Kumar A, Singh S, Kumar R, et al. Evaluation of thermo-fluidic performance of micro pulsating heat pipe with and without evaporator side surface structures[J]. Applied Thermal Engineering, 2024, 249.
[23] Diaz-Caraveo C, Wolk K, Miesner S, et al. Performance-Dryout Limits of Oscillating Heat Pipes: A Comprehensive Theoretical and Experimental Determination[J]. Journal of Thermophysics and Heat Transfer, 2025, 39(2): 289-99.
[24] Li Y X, Eldredge J D, Lavine A S, et al. A conjugate heat transfer model of oscillating heat pipe dynamics, performance, and dryout[J]. International Journal of Heat and Mass Transfer, 2024, 227.
[25] Parmar K, Parwani A K, Parmar N, et al. Identification of heat-transfer regime in closed-loop pulsating heat pipes via critical thermal analysis[J]. Journal of Thermal Analysis and Calorimetry, 2026.
[26] Singh A, Ghosh I. Numerical study of a cryogenic pulsating heat pipe for space applications[J]. International Communications in Heat and Mass Transfer, 2026, 178.
[27] Slobodeniuk M, Bertossi R, Ayel V, et al. Experimental study of the flat plate pulsating heat pipe operation during dry-out and flow re-activation periods under microgravity conditions[J]. International Journal of Multiphase Flow, 2022, 147.
[28] Liu Y, Yan Y H, Bao K L, et al. Effect of localized dry-out on startup and steady-state operation characteristics of ethanol-based oscillating heat pipes[J]. Applied Thermal Engineering, 2024, 257.
[29] Palani K C, Rajagopal D. Numerical modelling of dry-out in pulsating heat pipe using VOF model[J]. Journal of Mechanical Science and Technology, 2022, 36(8): 4279-87.
[30] Krambeck L, Domiciano K G, Betancur-Arboleda L A, et al. Novel flat plate pulsating heat pipe with ultra sharp grooves[J]. Applied Thermal Engineering, 2022, 211.
[31] Liu Y, Yan Y H, Wu X L, et al. A two-phase theoretical model incorporating liquid film dynamics for pulsating heat pipes[J]. International Journal of Heat and Mass Transfer, 2025, 245.
[32] Li Y X, Eldredge J D, Lavine A S, et al. A conjugate heat transfer model of oscillating heat pipe dynamics, performance, and dryout[J]. International Journal of Heat and Mass Transfer, 2024, 227.
[33] Li Y Y, Xiao Y X, Cheng C X, et al. Segmented thermal resistance model of flat-plate CLPHP based on PEMFC cooling[J]. International Journal of Hydrogen Energy, 2024, 56: 259-70.
[34] Li Y Y, Chang G F, Zhao W, et al. Start-up visualization and performance of flat-plate CLPHP based on PEMFC cooling[J]. International Journal of Heat and Mass Transfer, 2022, 190.
[35] Barua H, Ali M, Nuruzzaman M, et al. Effect of filling ratio on heat transfer characteristics and performance of a closed loop pulsating heat pipe[J]. Procedia Engineer, 2013, 56: 88-95.
[36] Rao Z H, Wang Q C, Zhao J T, et al. Experimental investigation on the thermal performance of a closed oscillating heat pipe in thermal management[J]. Heat Mass Transfer, 2017, 53(10): 3059-

71.
[37] Berdnikov V I, Gudim Y A. Thermodynamic model of ideal associated solutions with positive deviation from Raoult's law[J]. Steel in Translation, 2014, 44(9): 635-39.